Recovery of Brain Network Integration and Segregation During the Loss and Recovery of Consciousness Induced by Sevoflurane

Kangli Dong, Qishun Wei, Delin Zhang, Lu Zhang, Guozheng Wang, Xing Chen, and Jun Liu

***Abstract*— Anesthetic-induced loss of consciousness (LOC) has been studied using functional connectivity (FC) and functional network analysis (FNA), manifested as fragmentation of the whole-brain functional network. However, how the fragmented brain networks reversibly recover during the recovery of consciousness (ROC) remains vague. This study aims to investigate the changes in brain network structure during ROC, to better understand the network fragmentation during anesthesia, thus providing insights into consciousness monitoring. We analyzed EEG data recorded from 15 individuals anesthetized by sevoflurane. By investigating the properties of functional networks generated using different brain atlases and performing community detection for functional networks, we explored the changes in brain network structure to understand how fragmented brain networks recover during the ROC. We observed an overall larger FC magnitude during LOC than in the conscious state. The ROC was accompanied by the increasing binary network efficiency, decreasing FC magnitude, and decreasing community similarity with the functional atlas. Furthermore, we observed a negative correlation between modularity and community number ($p < 0.001$ and $BF_{10} > 4000$, linear regression test), in which modularity increased and community number decreased during ROC. Our results show that a larger FC magnitude reveals excessive synchronization of neuronal activities during LOC. The increasing binary network efficiency, decreasing community number, and decreasing community similarity indicate the recovery of functional network integration. The increasing modularity implies the recovery of functional network segregation during ROC. The results suggest the limitation of FC magnitude and modularity in monitoring anesthetized states and the potential of integrated information theory to evaluate consciousness.**

***Index Terms*— Anesthesia, consciousness, electroencephalogram, functional networks, community detection.**

I. Introduction

While much work on understanding the mechanism of anesthesia has focused on the molecular actions of various anesthetics on specific receptors at the cellular level [1], [2], changes in brain networks that result in unconscious network dynamics are still poorly understood [3]. A related and more comprehensive theory for anesthetic-induced unconsciousness is integrated information theory (IIT) [4], which holds that the balance between functional integration and segregation supports the existence of consciousness. Large-scale network studies of brain functional connectivity (FC) have revealed properties that facilitate the integration and segregation. For instance, the breakdown of FC represents the impaired connectivity between brain areas; modularity stands for the ability for specialized function to occur within densely interconnected groups of brain regions (segregation); characteristic path length and global efficiency in functional network analysis (FNA) represent the ability to rapidly combine segregation from distributed brain regions (integration) [5], [6]. FC and FNA provide insights into the neurological underpinnings of loss of consciousness (LOC) during anesthesia by evaluating the global and local structured behavior of brain networks [7], [8].

The breakdown of FC under sleep or anesthesia could be regarded as a feature of LOC, causing the impaired connectivity between brain areas [9], which is broadly consistent with the IIT of consciousness [4]. The studies using electroencephalography (EEG) and electrocorticography (ECOG) provided plentiful insights into the process of unconsciousness induced by anesthetics. For instance, Fabio et al. found that cortical effective connectivity is disturbed during midazolam-induced LOC [10] and non-rapid eye movement (NREM) sleep [11], and suggested that LOC may be characterized by a breakdown of cortical effective connectivity [10]. Using intracortical recordings in macaque monkeys, Schroeder et al. [12] showed that ketamine anesthesia inhibits communication among structurally linked cortical

Manuscript received 21 June 2022; revised 9 September 2022 and 3 October 2022; accepted 10 November 2022. Date of publication 14 November 2022; date of current version 31 January 2023. This work was supported in part by the National-Zhejiang Health Commission's Major S&T Project, under Grant WKJ-ZJ-2334; and in part by the National Key Research and Development Program of China under Grant 2019YFC1711800. *(Corresponding author: Jun Liu.)*

Kangli Dong, Qishun Wei, Guozheng Wang, and Xing Chen are with the Key Laboratory for Biomedical Engineering of Ministry of Education of China, Zhejiang University, Hangzhou 310027, China (e-mail: dongkl@zju.edu.cn; 22015026@zju.edu.cn; 21815093@zju.edu.cn; cnxingchen@zju.edu.cn).

Delin Zhang is with the Department of Anesthesiology, College of Medicine, The First Affiliated Hospital, Zhejiang University, Hangzhou 310027, China (e-mail: delin-zhang@zju.edu.cn).

Lu Zhang is with the Department of Rehabilitation, School of Medicine, Sir Run Run Shaw Hospital, Zhejiang University, Hangzhou 310027, China (e-mail: 3413037@zju.edu.cn).

Jun Liu is with the Key Laboratory for Biomedical Engineering of Ministry of Education of China, Zhejiang University, Hangzhou 310027, China, and also with the Research Institute of Zhejiang University-Taizhou, Taizhou 318012, China (e-mail: liujun@zju.edu.cn).

This article has supplementary downloadable material available at https://doi.org/10.1109/TNSRE.2022.3221965, provided by the authors.

Digital Object Identifier 10.1109/TNSRE.2022.3221965

regions. By investigating functional connectivity and constructing time-varying networks, Li et al. [13], [14] monitored the fluctuation of consciousness during anesthesia. Using network nodes (brain regions) and the FC between nodes, FNA provides a standard method to quantify and study functional integration and segregation of the brain. Using recorded rs-fMRI, Boly et al. [15] found an increase in modularity during human nonrapid eye movement sleep. During LOC induced by dexmedetomidine, Hashmi et al. [16] found an overall decline in network efficiency of the local and global functional networks. Specifically, the increasing modularity and decreasing efficiency of the functional network were considered to represent the reduced integrated ability of the brain during LOC, and the increasing modularity during anesthesia has been suggested to measure different states of consciousness [17].

Although significant progress has been obtained in understanding the cortical network fragmentation and neural correlates during anesthetic-induced LOC, how fragmented brain network reversibly recovers during the recovery of consciousness (ROC) induced by anesthetics is rarely mentioned. Based on theoretical models and empirical observations, studies have shown that the induction and recovery processes of anesthesia might be asymmetric, which can be seen as the phenomenon of anesthetic hysteresis [18], [19]. Although there have been studies employing EEG or ECoG in the recovery phase of anesthesia [20], [21], [22], the network-level mechanism of ROC induced by anesthetics is poorly understood. The detailed study of brain network structure during loss and recovery of consciousness would be of fundamental and translational scientific value. Scientifically, it would provide insight into our understanding of the brain network mechanisms of anesthetic-induced ROC. Clinically, it may provide insights into conscious state monitoring and anesthesia prognosis [23]. Specifically, it could examine the availability of these graph-theoretic indicators (i.e., FC magnitude, efficiency, modularity, etc.) monitoring different phases during anesthesia and develop more accurate methods for assessing consciousness.

This study aims to investigate the change in brain network properties (evaluated through graph-theoretical measures) and the community structure of brain networks during the loss and recovery of consciousness, thus gaining a better understanding of brain network fragmentation under anesthesia and provide insights into conscious state monitoring. Specifically, we focused on exploring global efficiency, which represents functional integration, and modularity, which represents functional segregation. On the basis of the modularity being estimated, we performed community detection to further investigate how fragmented communities of brain network recovers during anesthetic-induced ROC. The structure of the remaining sections is as follows: Section II introduces the research methods, including anesthetic protocol, EEG acquisition and source localization, construction of brain networks, graph-theoretical measures, and network community analysis. Section III firstly gives the results of graph-theoretical measures, then provides the results of network community analysis, including the community similarity analysis, the relationship between modularity versus community number, and the overall changes in community structure of functional networks. In Section IV, we discuss the implications of these results, suggesting the importance of functional atlas in anesthesia research and the potential of community number and IIT, not the FC and modularity to evaluate different states of consciousness.

II. Methods

A. Anesthetic Protocol and Participants

The anesthetic protocol and EEG collection were recently published in [24], in which the details of the anesthetic protocol could be found. EEG data from 15 patients under loss and recovery of consciousness induced by sevoflurane were included in this study. The data consists of 19 channels of EEG data from 7 males/8 females, aged 43.8 ± 13.4 years, weighing 63.3 ± 14.9 kilograms, and 165.8 ± 5.8 centimeters tall ($mean \pm SD$). The data collection was approved by the Ethics Committee of the first affiliated Hospital of Zhejiang University (Ethics No.: ChiCTR2000033139), and informed consent forms were signed with all patients before the data were collected.

B. EEG Data Acquisition and Preprocessing

EEG data were collected using ANT Neuro equipment with 19 channels: Fp1, Fp2, F7, F3, Fz, F4, F8, T7, C3, C4, T8, P7, P3, Pz, P4, P8, O1, and O2, with reference to M1 and M2 channels. The sampling rate was 1000 Hz. Electrolyte gel was used to decrease the electrode impedances to under $5k\Omega$. The EEG analysis was performed in MATLAB R2020a. Fig. 1 displays the general block diagram of EEG signal analysis. The DC bias correction, EEG filtering, power interference reduction, and average re-reference were performed using EEGLAB [25]. The bandpass filtering frequency range was 0.3 Hz to 50 Hz. To boost processing performance, the sample rate was decreased to 250 Hz. Normalized variance was used to identify abnormal signals with non-physiological artifacts, which were then manually rejected or retained by eye assessment. To decrease blinking and muscular activity artifacts, independent components analysis (ICA) was applied. For component selection and rejection, we used the artifacts chosen by ADJUST 1.1 [26]. Five EEG epochs (ETSev 2.0, 0.9, 0.6, 0.3, 0, which were selected based on the end-tidal sevoflurane concentration (ETSev in percentage) during anesthesia) from the loss and recovery of consciousness under sevoflurane-induced anesthesia were used for analysis, in which ETSev2.0 is the deep unconscious state (deep LOC), ETSev0 is the conscious state when patients were completely awake from anesthesia, ETSev0.9, 0.6 and 0.3 are intermediate states between deep unconscious and conscious states. Parts of the codes in this work are released on GitHub[1].

C. EEG Source Localization and Parcellation

Using the spherical approach in EEGLAB, the 19 channels were initially interpolated into 33 channels according to the 10–20 international system to ensure source localization accuracy. After that, the Beamformer algorithm [29] in

[1] https://github.com/Kangli-Dong

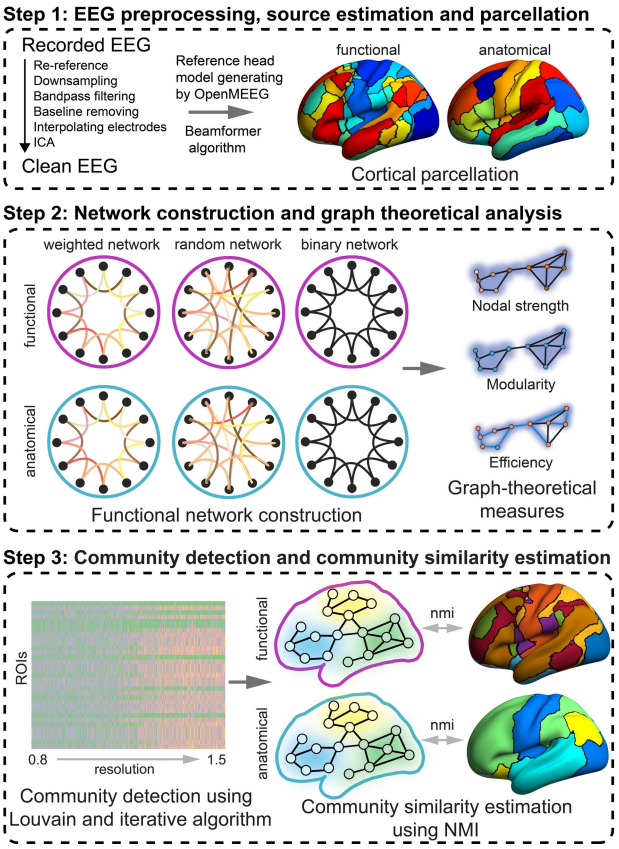

Fig. 1. Analysis framework. Step 1: EEG preprocessing, in which the recorded EEG was processed using re-reference, downsampling, bandpass filtering, baseline removing, interpolating electrodes, and ICA. Source localization, including reference head model generating and beamformer algorithm. Cortex parcellation using the Desikan-Killiany (anatomical) atlas [27] and Yeo (functional) atlas [28]. Step 2: Construction of weighted network, random network, and binary network. Evaluation of the graph-theoretical measures. Step 3: Community structure detection using Louvain algorithm and iterative community detection algorithm. Evaluation of similarity between community detection results and default divisions.

Brainstorm (Fig. 1. Step 1) [30] was used to carry out the source localization. Several reviews and articles [31], [32], [33], [34], [35], [36], [37], [38] acknowledge that even with low-density EEG settings (such as 19 electrodes), meaningful results of source estimation could be achieved. Details could be found in the supplementary material. We also provided the spectrum/spectral features and sensor-level network analysis (see Fig. S1 and S2 in the supplementary material) to prove the reliability of our work.

After source analysis of EEG, we segmented the voxels into 68 and 33 ROIs based on the Desikan-Killiany atlas [27] (a typical anatomical atlas) and Yeo brain atlas [28] (a typical functional atlas) as shown in Fig. 1. Step 1. We used the mean of all source signals in the ROI to represent its activity. The 68 and 33 ROIs belong to 4 and 8 default communities according to previous studies [28], [39], respectively (see Table. I and Table. II).

D. FC Estimation and Construction of Brain Functional Networks

To examine the change of network properties, we first constructed different functional networks under different conscious states during anesthesia, thus assessing the changes and correlations of the graph-theoretical measures of these networks in Sec II-E.

Drawing upon previous studies [17], [40], [41], [42], [43], we focused on the postprocessing of the alpha band. The alpha band of EEG was regarded as providing the most features to consciousness [17], [40] and dominant at surgical concentrations of anesthesia [41]. Furthermore, long-range integration during top-down processing (supports consciousness) appears to evolve with temporal dynamics of alpha band [42], [43]. We band-passed the source-level signals to obtain the alpha band (8-12 Hz). To evaluate the FC magnitude, we extracted the signal phase of alpha-band EEG using Hilbert transform, and then the Phase-locking values (PLV) [44] were employed as a connectivity measurement, which isolates the amplitudes and phases of the original signals for a certain frequency range and then calculates the phasic interrelationship between two signals:

$$PLV(t) = \frac{1}{n}\left|\sum_{i=1}^{n} e^{j\phi_i(t)}\right| \quad (1)$$

TABLE I
FUNCTIONAL BRAIN REGIONS ACCORDING TO YEO ATLAS

Networks	Regions
Visual	network1-left
	network1-right
	network2-left
	network2-right
Somotomotor	network3-left
	network3-right
	network4-left
	network4-right
DAN	network5-left
	network5-right
	network6-left
	network6-right
VAN	network7-left
	network7-right
Salience	network8-left
	network8-right
Limbic	network9-left
	network9-left
	network10-right
	network10-left
Control	network11-right
	network11-left
	network12-right
	network12-left
	network13-right
	network13-left
Default	network14-right
	network14-left
	network15-right
	network15-left
	network16-right
	network16-left
	network17

TABLE II
ANATOMIC BRAIN REGIONS ACCORDING TO DESIKAN-KILLIANY ATLAS

Networks	Regions
Sensory network	Cuneus
	Fusiform gyrus
	Insula
	Lateral occipital cortex
	Paracentral gyrus
	Pericalcarine cortex
	Postcentral gyrus
	Precentral gyrus
	Precuneus cortex
	Transverse temporal
Language/memory network	Bankssts
	Entorhinal
	Inferior temporal gyrus
	Lingual gyrus
	Middle temporal
	Parahippocampal gyrus
	Superior temporal gyrus
	Temporal pole
Attention/executive network	Caudal middle frontal gyrus
	Frontal pole
	Pars opercularis
	Pars orbitalis
	Pars triangularis
	Rostral middle frontal gyrus
	Superior frontal gyrus
	Superior parietal
	Supramarginal gyrus
Default mode network	Caudal anterior cingulate
	Inferior parietal
	isthmus cingulate
	lateral orbitofrontal
	medial orbitofrontal
	Posterior cingulate
	Rostral anterior cingulate

where $\phi_i(t)$ is the phase difference, n denotes the total number of trials. If the phase difference does not change much in the trial, then the PLV is close to 1, otherwise it is close to zero. PLV has several methodological advantages over other functional connectivity measures: Firstly, PLV evaluates the phase synchronization between two signals that only accounts for phase information, which makes PLV confounded of differences in amplitude. Secondly, PLV is a representative nonlinear coupling technique capable to obtain a statistical measure of functional connectivity, considering EEG source signals do not strictly satisfy the linearity assumption [45]. Simultaneously, PLV is computationally fast and could produce similar results for constructing EEG networks with nonlinear causal metric [46]. Thirdly, although PLV could be sensitive to volume conduction effects [45], [47], the source estimation addressed this problem. We used the mean PLV across all time-bins and epochs (2 seconds) as the FC measure of functional networks.

Then we constructed different weighted functional networks with two different scales (68 and 33 nodes), where each node represents each ROI and each edge represents the FC magnitude. After constructing the weighted functional networks, we transformed these weighted networks into binary networks and random networks by dealing with the edge weights, i.e., the FC magnitude, as shown in Step 2 in Fig. 1. To build the binary functional networks, we used a fixed edge density as a threshold, removed edges in the weighted networks with weights less than the threshold, and set the weights of edges greater than the threshold to 1. The random functional networks were constructed by disorganizing the small-world structure of the weighted networks using Brain Connectivity Toolbox (BCT) [5]. We also tested the influence of edge density on network properties by modulating it from 0.1 to 1. The binary functional networks with edge density = 0.2, 0.3, 0.4, 0.5 were kept for further analysis of community detection.

E. FNA: Graph-Theoretical Measures

Here we employed some graph-theoretical measures to examine the properties of the functional networks constructed in Sec. II-D, respectively. We examined the relationship between these network properties and sevoflurane concentration, thus exploring the network fragmentation and the brain's integrated ability during the loss and recovery of consciousness.

1) Measure of FC Magnitude: Nodal Strength k^W: We fist used nodal strength k^{W} to evaluate the FC magnitude (Fig. 1. Step 2). The nodal strength of node i in a weighted network is

$$k_i^{\mathrm{W}} = \sum_{j \in N} W_{ij} \tag{2}$$

where FC between i and j are associated with FC magnitude W_{ij}. The nodal strength k^{W} (edge density = 1) reflects the overall FC magnitude of a weighted network, which was calculated and visualized on brain surfaces for both Yeo and Desikan-Killiany atlas using ggseg package in R [48].

2) Measure of Network Segregation: Modularity: One of the most often used measures of functional segregation is modularity. The modularity measure quantifies the quality of modular partitions in such a way that the network has stronger connections inside a community or module, than across communities. The formulation of the modularity [49] of a binary network is:

$$Q = \frac{1}{l} \sum_{i,j \in N} \left(a_{ij} - \frac{k_i k_j}{l} \right) \delta_{m_i, m_j} \tag{3}$$

where m_i is the community containing node i, and $\delta_{m_i,m_j} = 1$ if $m_i = m_j$, and 0 otherwise; $l = \sum_{i,j \in N} a_{ij}$ is the number of links in a network.

The formulation of the modularity of a weighted network is

$$Q^{\mathrm{w}} = \frac{1}{l^w} \sum_{i,j \in N} \left[w_{ij} - \frac{k_i^w k_j^w}{l^w} \right] \delta_{m_i, m_j} \tag{4}$$

where $l^w = \sum_{i,j\in N} W_{ij}$ is the sum of all weights in a network.

Using Q maximizing, the network may be partitioned into non-overlapping communities or modules [49], [50]. The modularity (Fig. 1. Step 2) was estimated using the Louvain algorithm [50], which was made available via the Brain Connectivity Toolbox [5].

3) Measure of Network Integration: Global Efficiency: One of the most often cited measures of functional integration is global efficiency. The global network efficiency assesses global communication of the brain [51]. The global efficiency of a binary network can be calculated as follows:

$$E = \frac{1}{n}\sum_{i\in N} E_i = \frac{1}{n}\sum_{i\in N}\frac{\sum_{j\in N, j\neq i} d_{ij}^{-1}}{n-1} \tag{5}$$

where E_i is the efficiency of node i; $d_{ij} = \sum_{a_{uv}\in gi\leftrightarrow j} a_{uv}$ is the shortest path length (distance) between nodes i and j, $gi \leftrightarrow j$ is the shortest path (geodesic) between i and j. And $d_{ij} = \infty$ for all disconnected pairs i, j; n is the number of nodes.

The global efficiency of a weighted network is

$$E^{\mathrm{w}} = \frac{1}{n}\sum_{i\in N}\frac{\sum_{j\in N, j\neq i}\left(d_{ij}^{w}\right)^{-1}}{n-1} \tag{6}$$

where $d_{ij}^{w} = \sum_{a_{uv}\in \overset{W}{gi\leftrightarrow j}} f(W_{uv})$ is the shortest weighted path length between i and j; f is a map (e.g., an inverse) from weight to length; $gi \overset{W}{\leftrightarrow} j$ is the shortest weighted path between i and j. The global efficiency (Fig. 1. Step 2) was calculated using the Brain Connectivity Toolbox [5].

F. FNA: Network Community Analysis

We further performed community detection for functional networks using the Louvain algorithm and iterative community detection, thus exploring the changes in the community structure of brain networks and understanding how fragmented communities of brain network recovers during anesthesia-induced ROC.

1) Louvain Algorithm: Based on the estimation of modularity, we then explored the specific optimal community structure and the community number of binary functional networks under different conscious states using the Louvain algorithm (Fig. 1. Step 3). There are two steps in the Louvain algorithm for maximizing network modularity Q. In order to locate small communities inside a network, the algorithm first optimizes Q for local modularity. The algorithm then creates a new network whose nodes correspond to the communities discovered in the previous step. Self-loops represent links within communities discovered in the initial step of this new network, and the communities connected in the first step are represented by cross-node links whose weights are equal to the weights of the edges connecting the communities. To find large-scale communities, the Louvain algorithm optimizes Q of the new high-level network, and the process loops back to the initial step to re-optimize Q. For details of the Louvain algorithm, see [50].

2) Iterative Community Detection: The Louvain algorithm requires resolution to determine the rough scale of community structure. We used a robust detection algorithm [52] to identify the robust solution of the results obtained from the Louvain algorithm (Fig. 1. Step 3). The Iterative community discovery approach takes into account the usage of statistical null models to aid in the principled identification of structural communities in semi-decomposable systems. For details of iterative community detection, see [52]. We modulated the resolution in the Louvain algorithm from 0.8 to 1.5 with a step length of 0.01. For each resolution value (from 0.8 to 1.5), 100 repeated identification of community structure using the Louvain algorithm was executed to ensure the robustness of the results. All the results (800×100) were put into the robust detection algorithm to obtain a single community structure for each patient.

3) Normalized Mutual Information: After the community detection of functional networks, the similarity between community structure and default divisions (the divisions of brain regions into larger systems according to the atlases) could be evaluated. We quantified this similarity between community structures by using normalized mutual information (NMI) [53], [54] (Fig. 1. Step 3). An earlier description of the use of NMI measures for functional networks can be found in previous studies [53], [54], [55]. NMI can be calculated as follows:

$$\mathrm{NMI}(A,B) = \frac{-2\sum_{i=1}^{C_{\mathrm{A}}}\sum_{j=1}^{C_B} N_{ij}\log\left(\frac{N_{ij}N}{N_i N_j}\right)}{\sum_{i=1}^{C_{\mathrm{A}}} N_i \log\left(\frac{N_i}{N}\right) + \sum_{j=1}^{C_{\mathrm{B}}} N_j \log\left(\frac{N_j}{N}\right)} \tag{7}$$

where A and B are two partitions; The number of communities in partitions A and B is indicated by the symbol C_{A} and C_{B}, respectively. Both partitions have the same number of nodes, N. N_{ij} is the number of nodes that are shared by A and B's communities. Nodes of A's community i are totaled as N_i, and the number of nodes in B's community j is N_j. The NMI equals 0 when two partitions are completely independent and 1 when identical. The NMI of functional networks (averaged across edge densities = 0.2, 0.3, 0.4, 0.5) were kept for statistical analysis.

4) Community Ratio: To visualize and investigate the overall change in community structures, we averaged the functional network matrices of each conscious state across participants. Furthermore, the community structures detected by the Louvain algorithm and Iterative community detection were relabeled by maximizing the sum of the same labels to match the results of different conscious states. To assess the differences between community members during the change of consciousness state, we examined the proportion of each functional region in each community. The community ratio matrix was constructed and visualized using the heatmap in Seaborn (https://seaborn.pydata.org/). Results rendered in brain surfaces were visualized using BrainNet Viewer [56].

G. Statistical Analysis

To show the relationship between functional integration (represented by efficiency) and segregation (represented by modularity) and the relationship between modularity and

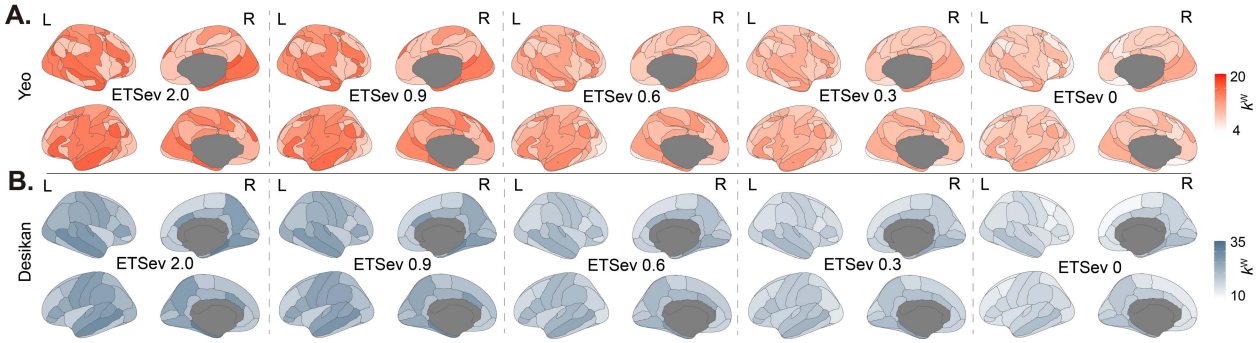

Fig. 2. Nodal strength k_i^W distribution of weighted functional networks (edge density = 1) constructed using Yeo and Desikan-Killiany atlas during the ROC from anesthesia. A: Nodal strength k_i^W of functional networks constructed using Yeo atlas during the ROC (from left to right: ETSev 2.0, ETSev 0.9, ETSev 0.6, ETSev 0.3, ETSev 0); B: Nodal strength k_i^W of weighted functional networks constructed using Desikan-Killiany atlas during the ROC (from left to right: ETSev 2.0, ETSev 0.9, ETSev 0.6, ETSev 0.3, ETSev 0); color bar stands for k_i^W scale of each brain region. It can be seen that the nodal strength k_i^W of weighted functional networks using Yeo and Desikan-Killiany atlas showed an overall decrease with the decrease of sevoflurane dose, which indicates the overall decrease of FC magnitude during the ROC from anesthesia.

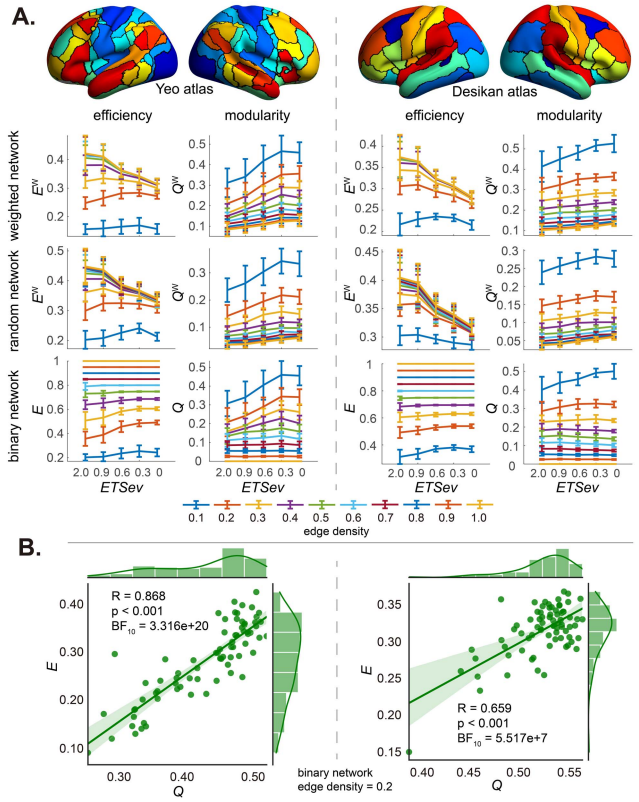

Fig. 3. The graph-theoretical measures (global efficiency and modularity) during the ROC from anesthesia. A: Variation trend of the graph-theoretical measures of different functional networks constructed using the Yeo brain atlas [28] (left panel), and Desikan-Killiany atlas [27] (right panel) with different edge densities (figures from the left column to right column: global efficiency, modularity; figures from the top row to bottom row: weighted network, random network, binary network); different edge densities were represented with different colors; B: Correlation diagram of efficiency E and modularity Q of the binary network (edge density = 0.2); left: result of network constructed using the Yeo atlas; right: result of network constructed using the Desikan-Killiany atlas. It can be seen that the efficiency E of the functional network (binary network) increased with the ROC despite the FC magnitude and the efficiency E of the weighted network decreased, and there is a significant positive correlation between modularity Q and global efficiency E.

community number, both conventional linear regression and Bayesian linear regression ($Bayesfactor = BF_{10}$) were used to verify the linear relationship between efficiency and modularity (Fig. 3. B), and the linear relationship between modularity and community number (Fig. 5. B–D and Table. III). The results (efficiency, modularity, community number) in all epochs (ETSev2.0, 0.9, 0.6, 0.3, 0) were used for calculating the correlation. The influence of confounding variables (sex, age, and ETSevs) in linear regression was excluded by building simple regression models ('regress out') for characteristic variables (efficiency, modularity, community number) and confounding variables, and keeping the residuals. $p<0.05$ and $BF_{10} > 100$ indicate strong evidence for a regression model. The JASP software package [57] was used to carry out the linear regression. The NMI data (Fig. 4) was tested by the repeated measures analysis of variance (ANOVA), and Bonferroni correction was used for the post-test. The ANOVA was employed using SPSS software version 23.0.

III. Results

In this section, we first demonstrated changes in graph-theoretical measures for the weighted, binary, and random functional networks to examine the change in network properties during the loss and recovery of consciousness in Section III-A. Considering FC magnitude affects the network structure according to the results in Section III-A, we further carried out community analysis for binary networks to verify the change in community structure of functional networks during the loss and recovery of consciousness (Section III-B, III-C, III-D). Specifically, we examined if there were dose-dependent effects in changing trend of community structures using different brain atlases in Section III-B, the relationship between modularity versus community number was displayed in Section III-C, and we visualized the overall changes in community structure of functional networks during the ROC in Section III-D.

A. Changes in Graph-Theoretical Measures (Nodal Strength, Modularity and Efficiency) of Functional Networks

We first examined the nodal strength distribution to show the change in the FC magnitude during anesthesia. Fig. 2

visualizes the nodal strength k_i^{W} distribution of weighted functional networks (edge density = 1) constructed using Yeo (Fig. 2. A) and Desikan-Killiany atlas (Fig. 2. B). The nodal strength k^{W} evaluates the averaged FC magnitude of a weighted network. We can see that the FC magnitude (nodal strength k_i^{W}) showed an overall decrease with the decrease of sevoflurane dose for both Yeo and Desikan-Killiany atlas.

Next, global efficiency and modularity of weighted, binary, and random functional networks were evaluated to discuss the change in network properties during the ROC from anesthesia. Fig. 3 displays the graph-theoretical measures (global efficiency and modularity) of functional networks during the loss and recovery of consciousness. Not consistent with previous work [58], [59], the decreased dose of sevoflurane was related to an overall decrease in FC magnitude, which could be demonstrated by the decreased global efficiency E^W of the random networks constructed using both Yeo and Desikan atlases during the ROC from anesthesia (Fig. 3. A). Furthermore, this result is compatible with the results of decreased nodal strength in Fig. 2. Additionally, an overall decrease in efficiency E^W of random and weighted networks was observed along with the decreased dose of sevoflurane (Fig. 3. A) for both Yeo and Desikan atlases, while an overall increase in efficiency E of binary networks was observed, which demonstrates that FNA with and without FC magnitude leads to opposite results. Furthermore, increased modularity of weighted, random (Q^W) and binary (Q) functional networks were observed (Fig. 3. A) for both Yeo and Desikan atlases. Efficiency E and modularity Q showed a significant positive correlation in binary functional networks (edge density = 0.2) constructed using both Yeo and Desikan atlases (Fig. 3. B. Yeo: R = 0.868, p < 0.001, BF_{10} = 3.316e+20; Desikan: R = 0.659, p < 0.001, BF_{10} = 5.517e+7) during the ROC from anesthesia, which was opposite to the results of some studies using fMRI [15], [60], but similar to the results of some studies using EEG [61]. To sum up, the global efficiency E of the functional network (binary network) increased despite the FC magnitude and the modularity (Q and Q^W) of the functional network decreased during the ROC from anesthesia.

B. Community Similarity of Brain Networks With Default Divisions

We then explored if there were differences in community structure change of brain networks constructed using different brain atlases during ROC. Using the community detection algorithm and NMI method, the community structure similarity with the default divisions of functional networks during ROC from anesthesia is displayed in Fig. 4. Firstly, for the functional networks constructed using Yeo atlas, an overall decrease of the averaged NMI was observed during the ROC from anesthesia (Fig. 4. A. p < 0.0001, F = 16.989, $Partial\ \eta^2 = 0.493$), indicating that the community structure of functional networks gradually deviated from the default division (Table. I), in other words, there was an increased communication among different functional regions during the ROC from anesthesia. For the functional networks constructed using Desikan-Killiany atlas, there was also a significant NMI change (Table. II) during the ROC from anesthesia

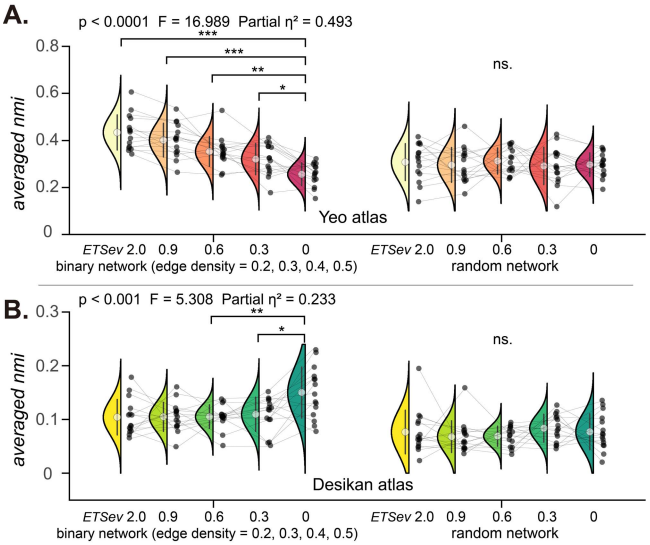

Fig. 4. Community similarity with default divisions (the divisions of brain regions into larger systems according to the atlases). A: NMI between community structures of patients' functional networks (averaged across edge densities = 0.2, 0.3, 0.4, 0.5) constructed using Yeo atlas during the ROC; B: NMI between community structures of patients' functional networks (averaged across edge densities = 0.2, 0.3, 0.4, 0.5) constructed using Desikan-Killiany atlas during the ROC. It can be seen that an overall decrease of NMI in functional networks constructed using Yeo atlas and no apparent trend of NMI in functional networks constructed using Desikan-Killiany atlas could be observed during the ROC from anesthesia.

(Fig. 4. B. p < 0.001, F = 5.308, $Partial\ \eta^2 = 0.233$), however, no apparent trend could be observed. The results of random networks demonstrate that the small-world structure of the functional networks was destroyed, therefore, no significant results could be observed (diagrams on the right in Fig. 4. A, B).

C. Relationship Between Modularity Versus Community Number

To explain the inconsistency between the decreased modularity during LOC and results from other studies, we tested the change of community number during the ROC from anesthesia. The binary network with edge density = 0.2 was used for analysis. Surprisingly, for functional networks constructed using Yeo atlas, an overall decrease in community number and increase in modularity Q were observed during ROC from anesthesia (Fig. 5. A). Furthermore, a significant negative correlation was observed between modularity and community number (Fig. 5. B. R = −0.872, p < 0.001, BF_{10} = 1.059e+21). We also carried out the statistical results of modularity and community number of the functional networks constructed using Desikan-Killiany atlas. An overall decrease in community number and increase in modularity Q were also observed during ROC from anesthesia (Fig. 5. C). Furthermore, a significant negative correlation between modularity and community number was also observed (Fig. 5. D. R = −0.593, p < 0.001, BF_{10} = 477623).

To prevent the impact of isolated nodes on the outcomes, the relationship between modularity and community number under different network edge densities using both Yeo and Desikan-Killiany atlas was tested by linear regression

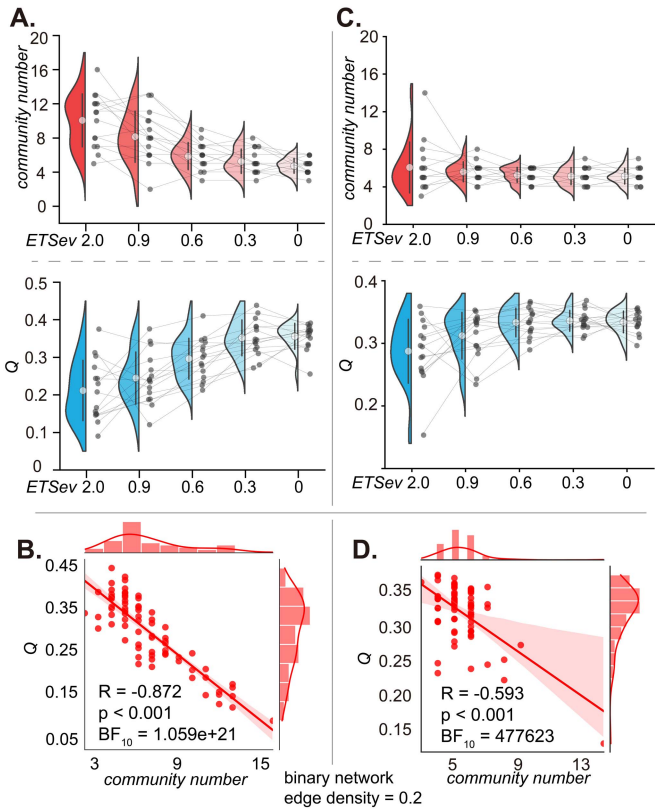

Fig. 5. Relationships between modularity Q and community number of the binary functional network with edge density = 0.2 during the ROC from anesthesia. A: Statistical diagrams of community number and modularity Q of functional networks constructed using Yeo atlas during the ROC from anesthesia; B: Correlation diagram between community number and modularity Q of functional networks constructed using Yeo atlas during the ROC from anesthesia; C: Statistical diagrams of community number and modularity Q of functional networks constructed using Desikan-Killiany atlas during the ROC from anesthesia; D: Correlation diagram between community number and modularity Q of functional networks constructed using Desikan-Killiany atlas during the ROC from anesthesia. It can be seen that for the functional networks constructed using both Yeo and Desikan-Killiany atlas, a significant negative correlation between community number and modularity Q was observed during the ROC from anesthesia.

(Table. III). The strong evidence for a regression ($p<0.001$ and $BF_{10}>4000$) model was provided (network edge density = 0.3, 0.4, 0.5), indicating the negative correlation between modularity and community number of functional networks during the ROC from anesthesia.

D. Overall Changes in Community Structure of Functional Networks

To visualize and investigate the overall change in community structure, we averaged the functional network matrices of each consciousness state across participants. The communities were relabeled by maximizing the sum of the same labels to match the results of different states of consciousness. Fig. 6 displays the community detection result of the functional networks constructed using Yeo atlas during the ROC from anesthesia. We ignored the analysis for the functional networks constructed using Desikan-Killiany atlas, considering no significant trend can be observed in the community similarity (Fig. 4. A). As can be seen from Fig. 6. A, the isolation of the left node of the visual network (community 1) was found during the loss and recovery of consciousness (ETSev 2.0, ETSev 0.9, ETSev 0.6, and ETSev 0.3 in Fig. 6. A). The heatmap of the community ratio could also display the isolation of the left node of the visual network (Fig. 6. B). Additionally, an overall decrease of communities with consistent functions (with consistent colors) was observed with the ROC. For instance, communities 1, 4, 6, 9, and 11 execute specialized function under ETSev 2.0; communities 1, 4, and 11 execute specialized function under ETSev 0.9; communities 1 and 11 execute specialized function under ETSev 0.6; communities 1 and 4 execute specialized function under ETSev 0.3 and 0, respectively (Fig. 6. A and B).

TABLE III
STATISTICAL RESULTS OF REGRESSION MODEL OF THE RELATIONSHIP BETWEEN MODULARITY Q AND COMMUNITY NUMBER UNDER DIFFERENT NETWORK EDGE DENSITIES USING BOTH YEO AND DESIKAN-KILLIANY ATLAS

Atlas	Edge density	p	R	BF_{10}
Yeo	0.3	<0.001	-0.839	5.089e+17
	0.4	<0.001	-0.617	2.323e+6
	0.5	<0.001	-0.613	1.841e+6
Desikan -Killiany	0.3	<0.001	-0.572	87253
	0.4	<0.001	-0.553	36822
	0.5	<0.001	-0.514	4597

IV. DISCUSSION

Anesthetic-induced unconsciousness has been studied using brain FC and FNA, which is attributed to the disruption of the brain's integrated ability. In this study, we investigated the change in brain network properties and the community structure of brain networks during the ROC to gain a better understanding of brain network fragmentation under anesthesia. Our results demonstrate that unconsciousness causes an excessive synchronization of neuronal activity, and the recovery of both functional network integration and segregation leads to the ROC induced by sevoflurane. We will discuss the implications of these findings below.

A. Sevoflurane Causes an Excessive Synchronization of Neuronal Activity and Cortical Network Fragmentation Simultaneously

The cortical network fragmentation could be revealed by two different phenomena: one is the breakdown of FC (the edge of the functional network) [10], [11], [12], [62], [63], and the other is the fragmentation of the network structure [15], [16], [59], [64]. Numerous studies have provided evidence for both meanings. However, some of the opposite results followed, e.g., the enhancement of the coherence [61], correlation [65], Granger causality [66], weighted phase lagging index (wPLI) [67] (contrary to the first meaning), and modularity without significant change [68], increased global efficiency index [69] (contrary to the second meaning). We also found increased FC magnitude in this study (Fig. 2). Bola et al. [65] supposed that excessive synchronization might represent unresponsive but conscious states. However, this assumption is not suitable for our study, considering consciousness was certainly

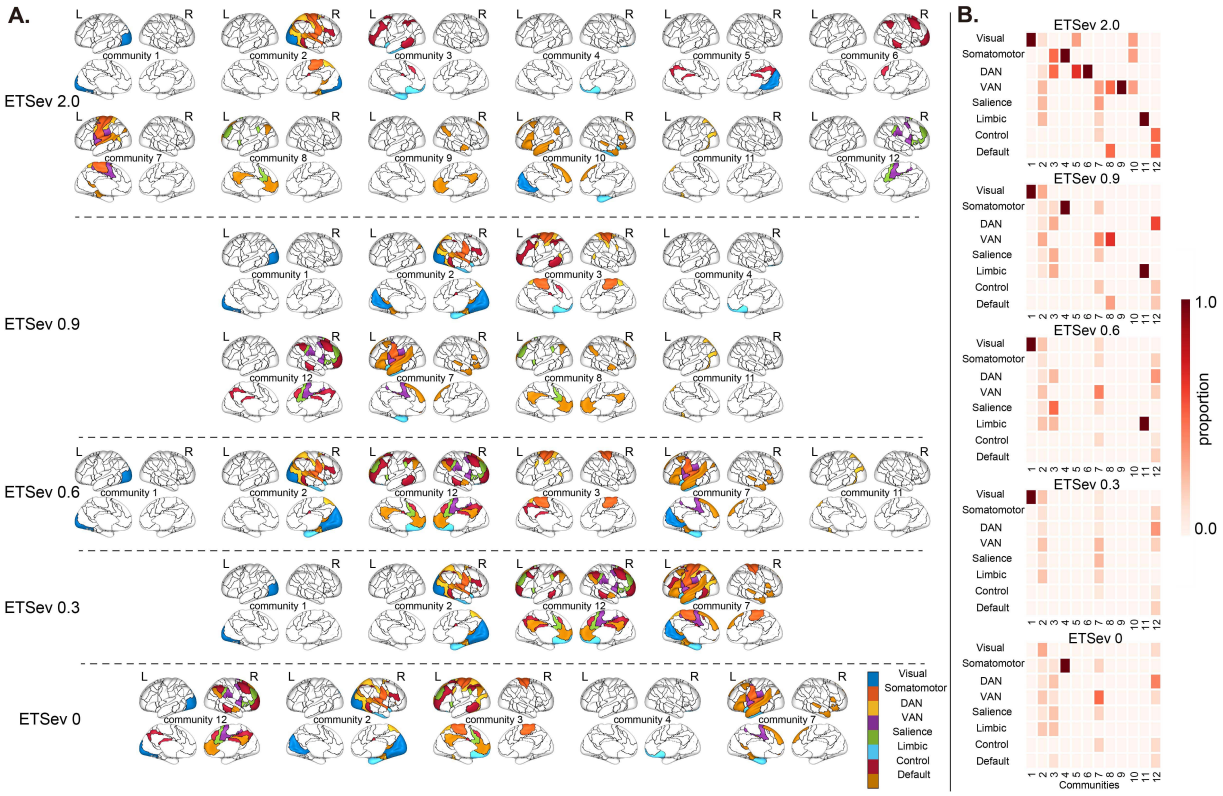

Fig. 6. The community detection result of the functional networks constructed using the Yeo atlas during the ROC from anesthesia (A: Topographic distribution of communities; brain regions with the same color are from the same community according to Yeo atlas; B: heatmap of the community ratio matrix; from top to bottom: ETSev 2.0, ETSev 0.9, ETSev 0.6, ETSev 0.3, ETSev 0; color bar stands for the absolute proportion scale of each functional region in each community). It can be seen that an overall decrease of communities with consistent colors (with consistent functions) was observed with the ROC from anesthesia, which indicates the restoration of communication among different functional regions.

refrained in clinical anesthesia. We believed that the increased connectivity [61], [65], [67] in our result is similar to the excessive synchronization observed in the unconsciousness during epilepsy [70], which also suggests that FC magnitude could not properly evaluate different anesthesia states. Furthermore, the lower global efficiency of the binary network during the LOC (Fig. 3) reveals the fragmentation of the cortical network, and the increased global efficiency index during the unconsciousness found in some studies [69] might be caused by the construction of a weighted functional network (Fig. 3). Overall, our result indicates that FC magnitude might not be suitable for evaluating consciousness, and the global efficiency of the binary functional network might be a better indicator.

B. Communication Among Functional, Rather Than Anatomical Regions Recovers During ROC

The parcellation atlas is the foundation of the construction of the functional network at the EEG source level and directly affects the interpretability of the results. A part of the studies using EEG stagnated at the sensor-level analysis [21], [69], [71], [72], which directly affected the definition of the functional network edge and its reliability. Some studies using both EEG and fMRI carried out the parcellation of the brain based on anatomical atlas [16], [73], which would reflect the anatomy of the brain well and adjust functional networks to a befitting size, but could not reflect the connectivity among functional regions of the brain. The ideal process of functional network construction should be using a functional atlas [64]. Hence, we investigated the influence of different cortical parcellation atlases (a typical anatomical atlas and a typical functional atlas) on the network properties and tracked the changes in community structure using NMI (Section III-B). The higher the NMI, the closer the network structure is to the default divisions, and the connections within the default communities are more frequent than the connections between different default communities, which indicates a lower functional integration. Therefore, with the decrease of sevoflurane dose, the community structure of the functional network (constructed using Yeo atlas) becomes more and more dissimilar to the default functional partition during anesthetic-induced loss and recovery of consciousness (Fig. 4 and 6), indicating an increased functional integration and communication between different functional regions, while the functional networks constructed using an anatomical atlas (Desikan-Killiany atlas) showed no apparent trends. The results indicate that the recovery functional integration and community structure during ROC is based on the functional division of the brain rather than the anatomy of the brain, and the consciousness is supported by the functional organization of the human cerebral cortex.

C. The Increasing Community Number, Rather Than Modularity, Could Be Used to Evaluate Anesthesia States

From the perspective of FNA and the direction of previous studies, network fragmentation can be reflected based on changes in network properties (e.g., the increase of modularity or number of communities [15], reduction in both local and

global network efficiency of functional networks [16], [64]) derived from thresholded FC matrices employing a fixed magnitude threshold [59]. Nevertheless, the results we displayed here (the decreased modularity and increased community number during unconsciousness under anesthesia (Fig. 5)) are inconsistent with previous studies. Modularity quantifies the benefits of community partitioning. A network with stronger connectivity between communities has smaller modularity than a network with stronger connectivity within communities. Modularity is one of the most commonly used measures of functional segregation, which should be used to measure the capacity of highly linked clusters of brain areas to perform specialized function [5]. The possible interpretation for the inconsistent results is that the changing trends of modularity, and community number are not necessarily consistent and the increased number of communities is a direct reflection of the fragmentation of a network. Although some work used increased modularity as a biomarker of unconsciousness [17], the result we showed (increasing modularity during ROC) indicates that modularity could not be used to evaluate anesthesia states while community number is a more appropriate measure.

D. The Potential of IIT to Evaluate Conscious States Under Anesthesia

Overall, all the network metrics discussed above reflect the functional integration or segregation defined in the IIT [4], which claims that consciousness is supported by a balance of integration and segregation. IIT is a conceptual framework of consciousness associated with anesthesia-induced unconsciousness. A lot of work has started to find evidence for IIT using different neuroimaging and analysis methods. Using state-space reconstruction for conscious states, Lee et al. [74] proposed that inducing general anesthesia with propofol impairs the brain's integrated ability. During propofol-induced unconsciousness, Liang et al. [75] reported a loss of efficient global communication capacity but a rise in local functional segregation in the cortical network. When compared to controls, Rizkallah et al. [76] found that functional networks in participants with disorders of consciousness (DOC) exhibited less integration and more segregation. Using phase-amplitude coupling (PAC) analysis, propofol was found to cause neuronal populations to become 'busy' on a local scale, limiting functional integration in long-range areas, according to Liang et al. [77]. In a recent study, Dong et al. [24] also explored the integration and segregation using the PAC on multiple spatial scales. Here we show in this study, the increased global efficiency and modularity (Fig. 3), decreased community similarity of brain networks with default divisions (Fig. 4 and 6), and decreased community number (Fig. 5) of binary functional networks during the ROC from anesthesia, all together reveal the recovery of functional network integration and segregation from the perspective of brain network structure. Therefore, IIT has great potential for evaluating consciousness. FC and FNA should be used in anesthesia research from the perspective of integration and segregation, which is expected to lead to the development of anesthesia monitoring.

E. Defects and Future Directions

Firstly, although recent investigations confirmed the capability of recreating the source using low-density EEG data [31], [32], [33], [34], [35], [36], [37], [38], high-density EEG settings are always preferable and low-density EEG collection is a serious limitation of this study. We hope that we can obtain more reliable results using high-density EEG collection in future studies. Secondly, we track network changes by steadily increasing or decreasing propofol or sevoflurane doses rather than adopting a randomized sequence or alternating decreased and increased doses, which may be impractical given participant safety. Thirdly, the small sample size and incomplete data (especially for the induction process) limited the interpretability of the results. The data set has only 15 patients, which might have led to inconsistent findings. Fourthly, resting-state EEG-based functional networks were used to evaluate the integration and segregation of the brain, however, actual causal interaction associated with the IIT should be tested using high-dimensional responses of the brain to perturbations [78], [79]. Therefore, actual causal interaction can not be measured in this study, which only evaluated the potential global and local structured behavior of the brain network using statistical techniques.

For future consideration, additional types of FC should be considered to verify the conclusion of this study. Moreover, the high-density EEG acquisition should cover the whole anesthesia process, and task-state should be considered in brain network study under anesthesia. Finally, the dynamic FC analysis can improve our comprehension of the dynamic change process of the whole-brain network.

V. Conclusion

The inability of the brain to integrate and segregate processing, which is generally manifested as a fragmentation of the whole-brain functional network, is one of the most recognized neural mechanisms of LOC. Insight into brain network mechanisms of ROC induced by anesthetics can be gained from a systematic study of the brain network properties and community structure. As shown above, an overall larger FC magnitude and weighted network efficiency but lower binary network efficiency during sevoflurane-induced LOC were observed. Community similarity among functional rather than anatomical regions is reduced during ROC. Furthermore, a negative correlation between modularity versus community number was observed. Taking the IIT theory as the foothold, these findings demonstrate that unconsciousness causes an excessive synchronization of neuronal activity, and the recovery of both functional network integration and segregation leads to ROC. The use of FC and modularity to evaluate anesthetic states needs to be re-examined, and assessing the integration-segregation balance should be further utilized in future directions.

References

[1] E. N. Brown, P. L. Purdon, and C. J. Van Dort, "General anesthesia and altered states of arousal: A systems neuroscience analysis," *Annu. Rev. Neurosci.*, vol. 34, no. 1, pp. 601–628, Jul. 2011.

[2] N. P. Franks, "General anaesthesia: From molecular targets to neuronal pathways of sleep and arousal," *Nature Rev. Neurosci.*, vol. 9, pp. 370–386, May 2008.

[3] M. T. Alkire, A. G. Hudetz, and G. Tononi, "Consciousness and anesthesia," *Science*, vol. 322, no. 5903, pp. 876–880, 2008.

[4] G. Tononi, "An information integration theory of consciousness," *BMC Neurosci.*, vol. 5, no. 1, pp. 1–22, 2004.

[5] M. Rubinov and O. Sporns, "Complex network measures of brain connectivity: Uses and interpretations," *NeuroImage*, vol. 52, no. 3, pp. 1059–1069, Apr. 2010.

[6] O. Sporns, "Network attributes for segregation and integration in the human brain," *Current Opinion Neurobiol.*, vol. 23, no. 2, pp. 162–171, Apr. 2013.

[7] M. Alkire, "Probing the mind: Anesthesia and neuroimaging," *Clin. Pharmacol. Therapeutics*, vol. 84, no. 1, pp. 149–152, Jul. 2008.

[8] J. Liu et al., "Progress of brain network studies on anesthesia and consciousness: Framework and clinical applications," *Engineering*, Dec. 2021.

[9] G. A. Mashour, "Cognitive unbinding: A neuroscientific paradigm of general anesthesia and related states of unconsciousness," *Neurosci. Biobehavioral Rev.*, vol. 37, no. 10, pp. 2751–2759, Dec. 2013.

[10] F. Ferrarelli et al., "Breakdown in cortical effective connectivity during midazolam-induced loss of consciousness," *Proc. Nat. Acad. Sci. USA*, vol. 107, no. 6, pp. 2681–2686, 2010.

[11] M. Massimini et al., "Triggering sleep slow waves by transcranial magnetic stimulation," *Proc. Nat. Acad. Sci. USA*, vol. 104, no. 20, pp. 8496–8501, 2007.

[12] K. E. Schroeder et al., "Disruption of corticocortical information transfer during ketamine anesthesia in the primate brain," *NeuroImage*, vol. 134, pp. 459–465, Jul. 2016.

[13] F. Li et al., "Identification of the general anesthesia induced loss of consciousness by cross fuzzy entropy-based brain network," *IEEE Trans. Neural Syst. Rehabil. Eng.*, vol. 29, pp. 2281–2291, 2021.

[14] Y. Li et al., "Recognition of general anesthesia-induced loss of consciousness based on the spatial pattern of the brain networks," *J. Neural Eng.*, vol. 18, no. 5, p. 056039, 2021.

[15] M. Boly et al., "Hierarchical clustering of brain activity during human nonrapid eye movement sleep," *Proc. Nat. Acad. Sci. USA*, vol. 109, no. 15, pp. 5856–5861, 2012.

[16] J. A. Hashmi et al., "Dexmedetomidine disrupts the local and global efficiencies of large-scale brain networks," *Anesthesiology*, vol. 126, no. 3, pp. 419–430, 2017.

[17] K. Hyoungkyu, A. G. Hudetz, L. Joseph, G. A. Mashour, and L. Uncheol, "Estimating the integrated information measure phi from high-density electroencephalography during states of consciousness in humans," *Frontiers Hum. Neurosci.*, vol. 12, p. 42, Feb. 2018.

[18] Z. Huang et al., "Asymmetric neural dynamics characterize loss and recovery of consciousness," *NeuroImage*, vol. 236, Aug. 2021, Art. no. 118042.

[19] M. L. Steyn-Ross, D. A. Steyn-Ross, and J. W. Sleigh, "Modelling general anaesthesia as a first-order phase transition in the cortex," *Prog. Biophys. Mol. Biol.*, vol. 85, nos. 2–3, pp. 369–385, Jun. 2004.

[20] J. D. Breshears et al., "Stable and dynamic cortical electrophysiology of induction and emergence with propofol anesthesia," *Proc. Nat. Acad. Sci. USA*, vol. 107, no. 49, pp. 21170–21175, 2010.

[21] P. L. Purdon et al., "Electroencephalogram signatures of loss and recovery of consciousness from propofol," *Proc. Nat. Acad. Sci. USA*, vol. 110, no. 12, pp. E1142–E1151, 2013.

[22] C. E. Warnaby, J. W. Sleigh, D. Hight, S. Jbabdi, and I. Tracey, "Investigation of slow-wave activity saturation during surgical anesthesia reveals a signature of neural inertia in humans," *Anesthesiology*, vol. 127, no. 4, pp. 645–657, Oct. 2017.

[23] G. A. Mashour et al., "Recovery of consciousness and cognition after general anesthesia in humans," *Elife*, vol. 10, p. e59525, May 2021.

[24] K. Dong et al., "Intrinsic phase-amplitude coupling on multiple spatial scales during the loss and recovery of consciousness," *Comput. Biol. Med.*, vol. 147, Jul. 2022, Art. no. 105687.

[25] A. Delorme and S. Makeig, "EEGLAB: An open source toolbox for analysis of single-trial EEG dynamics including independent component analysis," *J. Neurosci. Methods*, vol. 134, no. 1, pp. 9–21, Mar. 2004.

[26] A. Mognon, J. Jovicich, L. Bruzzone, and M. Buiatti, "ADJUST: An automatic EEG artifact detector based on the joint use of spatial and temporal features," *Psychophysiology*, vol. 48, no. 2, pp. 229–240, Feb. 2011.

[27] R. S. Desikan et al., "An automated labeling system for subdividing the human cerebral cortex on MRI scans into gyral based regions of interest," *NeuroImage*, vol. 31, no. 3, pp. 968–980, 2006.

[28] B. T. Yeo et al., "The organization of the human cerebral cortex estimated by intrinsic functional connectivity," *J. Neurophysiol.*, vol. 106, no. 3, pp. 1125–1165, Sep. 2011.

[29] R. D. Pascual-Marqui, C. M. Michel, and D. Lehmann, "Low resolution electromagnetic tomography: A new method for localizing electrical activity in the brain," *Int. J. Psychophysiol.*, vol. 18, no. 1, pp. 49–65, Oct. 1994.

[30] S. Baillet, K. Friston, and R. Oostenveld, "Academic software applications for electromagnetic brain mapping using MEG and EEG," *Comput. Intell. Neurosci.*, vol. 2011, Jan. 2011, Art. no. 972050.

[31] C. M. Michel and D. Brunet, "EEG source imaging: A practical review of the analysis steps," *Frontiers Neurol.*, vol. 10, p. 325, Apr. 2019.

[32] P. Sharma et al., "Ictal and interictal electric source imaging in presurgical evaluation: A prospective study," *Eur. J. Neurol.*, vol. 25, no. 9, pp. 1154–1160, 2018.

[33] L. Ding, G. A. Worrell, T. D. Lagerlund, and B. He, "Ictal source analysis: Localization and imaging of causal interactions in humans," *Neuroimage*, vol. 34, pp. 575–586, Jan. 2007.

[34] F. Sperli, L. Spinelli, M. Seeck, M. Kurian, C. M. Michel, and G. Lantz, "EEG source imaging in pediatric epilepsy surgery: A new perspective in presurgical workup," *Epilepsia*, vol. 47, no. 6, pp. 981–990, Jun. 2006.

[35] J. Song et al., "EEG source localization: Sensor density and head surface coverage," *J. Neurosci. methods*, vol. 256, pp. 9–21, Dec. 2015.

[36] C. M. Michel and B. He, "EEG source localization," *Handbook Clin. Neurol.*, vol. 160, pp. 85–101, Jan. 2019.

[37] A. G. Baroumand et al., "Automated eeg source imaging: A retrospective, blinded clinical validation study," *Clin. Neurophysiol.*, vol. 129, no. 11, pp. 2403–2410, 2018.

[38] D. A. Nguyen-Danse, S. Singaravelu, L. A. S. Chauvigné, A. Mottaz, L. Allaman, and A. G. Guggisberg, "Feasibility of reconstructing source functional connectivity with low-density EEG," *Brain Topography*, vol. 34, no. 6, pp. 709–719, Nov. 2021.

[39] Y. Zhang, C. Wang, Y. Wang, F. Yan, Q. Wang, and L. Huang, "Investigating dynamic functional network patterns after propofol-induced loss of consciousness," *Clin. Neurophysiol.*, vol. 130, no. 3, pp. 331–340, Mar. 2019.

[40] J.-Y. Moon, U. Lee, S. Blain-Moraes, and G. A. Mashour, "General relationship of global topology, local dynamics, and directionality in large-scale brain networks," *PLOS Comput. Biol.*, vol. 11, no. 4, Apr. 2015, Art. no. e1004225.

[41] S. Hagihira, "Changes in the electroencephalogram during anaesthesia and their physiological basis," *Brit. J. Anaesthesia*, vol. 115, pp. i27–i31, Jul. 2015.

[42] A. von Stein and J. Sarnthein, "Different frequencies for different scales of cortical integration: From local gamma to long range alpha/theta synchronization," *Int. J. Psychophysiol.*, vol. 38, no. 3, pp. 301–313, 2000.

[43] M. Del Carmen Herrojo Ruiz, S. Koelsch, and J. Bhattacharya, "Different scales of cortical integration during the processing of musical syntax: From early long-range alpha phase synchronization to late local gamma oscillations," in *Proc. Annu. Meeting Cogn. Neurosci. Soc. (CNS)*, 2007.

[44] J. P. Lachaux, E. Rodriguez, J. Martinerie, and F. J. Varela, "Measuring phase synchrony in brain signals," *Hum. Brain Mapping*, vol. 8, no. 4, pp. 194–208, Jan. 1999.

[45] V. Sakkalis, "Review of advanced techniques for the estimation of brain connectivity measured with EEG/MEG," *Comput. Biol. Med.*, vol. 41, no. 12, pp. 1110–1117, 2011.

[46] C. Beauchene, S. Roy, R. Moran, A. Leonessa, and N. Abaid, "Comparing brain connectivity metrics: A didactic tutorial with a toy model and experimental data," *J. Neural Eng.*, vol. 15, no. 5, Oct. 2018, Art. no. 056031.

[47] I. B. Islam et al., "Recent trends in non-invasive neural recording based brain-to-brain synchrony analysis on multidisciplinary human interactions for understanding brain dynamics: A systematic review," *Frontiers Comput. Neurosci.*, vol. 16, p. 51, Jun. 2022, Art. no. 875282.

[48] A. M. Mowinckel and D. Vidal-Piñeiro, "Visualization of brain statistics with R packages *ggseg* and *ggseg3d*," *Adv. Methods Practices Psychol. Sci.*, vol. 3, no. 4, pp. 466–483, Dec. 2020.

[49] M. E. J. Newman, "Modularity and community structure in networks," *Proc. Nat. Acad. Sci. USA*, vol. 103, no. 23, pp. 8577–8582, 2006.

[50] V. D. Blondel, J.-L. Guillaume, R. Lambiotte, and E. Lefebvre, "Fast unfolding of communities in large networks," *J. Stat. Mech., Theory Exp.*, vol. 2008, no. 10, Oct. 2008, Art. no. P10008.
[51] V. Latora and M. Marchiori, "Efficient behavior of small-world networks," *Phys. Rev. Lett.*, vol. 87, Oct. 2001, Art. no. 198701.
[52] D. S. Bassett, M. A. Porter, N. F. Wymbs, S. T. Grafton, J. M. Carlson, and P. J. Mucha, "Robust detection of dynamic community structure in networks," *Chaos, Interdiscipl. J. Nonlinear Sci.*, vol. 23, no. 1, Mar. 2013, Art. no. 013142.
[53] A. Alexander-Bloch, R. Lambiotte, B. Roberts, J. Giedd, N. Gogtay, and E. Bullmore, "The discovery of population differences in network community structure: New methods and applications to brain functional networks in schizophrenia," *NeuroImage*, vol. 59, no. 4, pp. 3889–3900, Feb. 2012.
[54] N. Xuan, V. Julien, S. Wales, and J. Bailey, "Information theoretic measures for clusterings comparison: Variants, properties, normalization and correction for chance," *J. Mach. Learn. Res.*, vol. 11, pp. 2837–2854, Oct. 2010.
[55] T. E. Larkin et al., "Altered network architecture of functional brain communities in chronic nociplastic pain," *NeuroImage*, vol. 226, Feb. 2021, Art. no. 117504.
[56] M. Xia, J. Wang, and Y. He, "BrainNet viewer: A network visualization tool for human brain connectomics," *PLoS ONE*, vol. 8, no. 7, Jul. 2013, Art. no. e68910.
[57] J. Love et al., "JASP: Graphical statistical software for common statistical designs," *J. Stat. Softw.*, vol. 88, pp. 1–17, Jan. 2019.
[58] H. Xie et al., "Differential effects of anesthetics on resting state functional connectivity in the mouse," *J. Cerebral Blood Flow Metabolism*, vol. 40, no. 4, pp. 875–884, 2020.
[59] C. N. Areshenkoff et al., "Muting, not fragmentation, of functional brain networks under general anesthesia," *NeuroImage*, vol. 231, May 2021, Art. no. 117830.
[60] R. M. Hutchison, M. Hutchison, K. Y. Manning, R. S. Menon, and S. Everling, "Isoflurane induces dose-dependent alterations in the cortical connectivity profiles and dynamic properties of the brain's functional architecture," *Hum. Brain Mapping*, vol. 35, no. 12, pp. 5754–5775, Dec. 2014.
[61] R. M. Pullon, L. Yan, J. W. Sleigh, and C. E. Warnaby, "Granger causality of the electroencephalogram reveals abrupt global loss of cortical information flow during propofol-induced loss of responsiveness," *Anesthesiology*, vol. 133, no. 4, pp. 774–786, Oct. 2020.
[62] D. Krzemiński, M. Kamiński, A. Marchewka, and M. Bola, "Breakdown of long-range temporal correlations in brain oscillations during general anesthesia," *NeuroImage*, vol. 159, pp. 146–158, Oct. 2017.
[63] M. Massimini, F. Ferrarelli, R. Huber, S. K. Esser, H. Singh, and G. Tononi, "Breakdown of cortical effective connectivity during sleep," *Science*, vol. 309, no. 5744, pp. 2228–2232, Sep. 2005.
[64] M. M. Monti et al., "Dynamic change of global and local information processing in propofol-induced loss and recovery of consciousness," *PLoS Comput. Biol.*, vol. 9, no. 10, Oct. 2013, Art. no. e1003271.
[65] M. Bola, A. B. Barrett, A. Pigorini, L. Nobili, A. K. Seth, and A. Marchewka, "Loss of consciousness is related to hyper-correlated gamma-band activity in anesthetized macaques and sleeping humans," *NeuroImage*, vol. 167, pp. 130–142, Feb. 2018.
[66] A. B. Barrett et al., "Granger causality analysis of steady-state electroencephalographic signals during propofol-induced anaesthesia," *PLoS ONE*, vol. 7, no. 1, Jan. 2012, Art. no. e29072.
[67] P. E. Vlisides et al., "Dynamic cortical connectivity during general anesthesia in surgical patients," *Anesthesiology*, vol. 130, no. 6, pp. 885–897, 2019.
[68] T. Uehara et al., "Efficiency of a 'small-world' brain network depends on consciousness level: A resting-state fMRI study," *Cerebral Cortex*, vol. 24, no. 6, pp. 1529–1539, 2014.
[69] D. Sattin et al., "Analyzing the loss and the recovery of consciousness: Functional connectivity patterns and changes in heart rate variability during propofol-induced anesthesia," *Frontiers Syst. Neurosci.*, vol. 15, Apr. 2021, Art. no. 652080.
[70] M. Arthuis et al., "Impaired consciousness during temporal lobe seizures is related to increased long-distance cortical–subcortical synchronization," *Brain*, vol. 132, no. 8, pp. 2091–2101, 2009.
[71] E. A. Mukamel, K. F. Wong, M. J. Prerau, E. N. Brown, and P. L. Purdon, "Phase-based measures of cross-frequency coupling in brain electrical dynamics under general anesthesia," in *Proc. Annu. Int. Conf. IEEE Eng. Med. Biol. Soc.*, Aug. 2011, pp. 1981–1984.
[72] S. Chennu, S. O'Connor, R. Adapa, D. K. Menon, and T. A. Bekinschtein, "Brain connectivity dissociates responsiveness from drug exposure during propofol-induced transitions of consciousness," *PLOS Comput. Biol.*, vol. 12, no. 1, Jan. 2016, Art. no. e1004669.
[73] S. Blain-Moraes et al., "Network efficiency and posterior alpha patterns are markers of recovery from general anesthesia: A high-density electroencephalography study in healthy volunteers," *Frontiers Hum. Neurosci.*, vol. 11, p. 328, Jan. 2017.
[74] U. Lee, G. A. Mashour, S. Kim, G.-J. Noh, and B.-M. Choi, "Propofol induction reduces the capacity for neural information integration: Implications for the mechanism of consciousness and general anesthesia," *Consciousness Cognition*, vol. 18, no. 1, pp. 56–64, Mar. 2009.
[75] Z. Liang et al., "Information integration and mesoscopic cortical connectivity during propofol anesthesia," *Anesthesiology*, vol. 132, no. 3, pp. 504–524, 2020.
[76] J. Rizkallah et al., "Decreased integration of EEG source-space networks in disorders of consciousness," *NeuroImage, Clin.*, vol. 23, Jan. 2019, Art. no. 101841.
[77] Z. Liang, X. Jin, Y. Ren, T. Yu, and X. Li, "Propofol anesthesia decreased the efficiency of long-range cortical interaction in humans," *IEEE Trans. Biomed. Eng.*, vol. 69, no. 1, pp. 165–175, Jan. 2021.
[78] M. Oizumi, L. Albantakis, and G. Tononi, "From the phenomenology to the mechanisms of consciousness: Integrated information theory 3.0," *PLoS Comput. Biol.*, vol. 10, no. 5, May 2014, Art. no. e1003588.
[79] D. M. A. Mehler and K. P. Kording, "The lure of misleading causal statements in functional connectivity research," 2018, *arXiv:1812.03363*.